SURFACE STRUCTURES AND SURFACE PROCESSES OF CERAMICS WITH ATOMIC RESOLUTION - A STUDY BY SCANNING TUNNELING MICROSCOPY

FINAL REPORT

IGNATIUS S.T. TSONG
WILLIAM T. PETUSKEY

DECEMBER 10, 1991

U.S. ARMY RESEARCH OFFICE

CONTRACT NO. DAAL03-88-K-0098

ARIZONA STATE UNIVERSITY

APPROVED FOR PUBLIC RELEASE:
DISTRIBUTION UNLIMITED.

MASTER COPY KEEP THIS COPY FOR REPRODUCTION PURPOSES

REPORT DOCUMENTATION PAGE

Form Approved
OMB No 0704-0188

1. AGENCY USE ONLY (Leave blank)	2. REPORT DATE	3. REPORT TYPE AND DATES COVERED
	10 December 1991	Final, 1 June 1988 - 30 September 1991

4. TITLE AND SUBTITLE

Surface structures and surface processes of ceramics with atomic resolution-a study by scanning tunneling microscopy

5. FUNDING NUMBERS

DAAL03-88-K-0098

6. AUTHOR(S)

Ignatius S.T. Tsong
William T. Petuskey

7. PERFORMING ORGANIZATION NAME(S) AND ADDRESS(ES)

Arizona State University
Tempe, AZ 85287

8. PERFORMING ORGANIZATION REPORT NUMBER

9. SPONSORING / MONITORING AGENCY NAME(S) AND ADDRESS(ES)

U. S. Army Research Office
P. O. Box 12211
Research Triangle Park, NC 27709-2211

10. SPONSORING / MONITORING AGENCY REPORT NUMBER

ARO 24845.15-MS

11. SUPPLEMENTARY NOTES

The view, opinions and/or findings contained in this report are those of the author(s) and should not be construed as an official Department of the Army position, policy, or decision, unless so designated by other documentation.

12a. DISTRIBUTION / AVAILABILITY STATEMENT

Approved for public release; distribution unlimited.

12b. DISTRIBUTION CODE

13. ABSTRACT *(Maximum 200 words)*

We applied a new technique for surface imaging, scanning tunneling microscopy (STM), to study the atomic and electronic structures of ceramic surfaces. The model ceramic chosen for this study was SiC. STM imaging was possible when the SiC single crystals were doped with nitrogen to render them semiconducting. Atomically resolved images were successfully taken on surfaces of cubic β-SiC(100) and (111), which showed a variety of reconstructions. In particular, the STM images of the β-SiC(111) surface showed a 6 x 6 geometry, in contrast to a $6\sqrt{3}$ x $6\sqrt{3}$ geometry when measured by low-energy electron diffraction (LEED). We found that this discrepancy was due to a graphite monolayer incommensurately grown on top of the Si-terminated β-SiC(111) surface. This conclusion was reached after probing the electronic structure of the surface by scanning tunneling spectroscopy (STS). On a larger scale, i.e. over distances between 50 nm and 500 nm, the surface topographics observed by STM were correlated with the initial growth modes of the SiC simple crystals. In addition to the STM studies, we conducted experimental and theoretical investigations on the thermochemistry and interfacial displacement reactions of the Ti-Si-C and Ti-Si-N systems in order to refine the understanding of thermodynamic and phase equilibria characteristics of ceramic-metal composite systems.

14. SUBJECT TERMS

15. NUMBER OF PAGES

16. PRICE CODE

17. SECURITY CLASSIFICATION OF REPORT	18. SECURITY CLASSIFICATION OF THIS PAGE	19. SECURITY CLASSIFICATION OF ABSTRACT	20. LIMITATION OF ABSTRACT
UNCLASSIFIED	UNCLASSIFIED	UNCLASSIFIED	UL

TABLE OF CONTENTS

		Page
I.	Statement of the Problem	1
II.	Summary of the Most Important Results	1
	II.1 STM Studies of the β-SiC(100) Surface	1
	II.2 STM Studies of the β-SiC(111) Surface	2
	II.3 STM Studies of β-SiC(111) and α-SiC(0001) Surfaces Under External Stresses	5
	II.4 Physical Chemistry and Reaction Chemistry of SiC Ceramics	5
III.	Publications List	8
	III.1 Papers Published, In Press, and Submitted	8
	III.2 Ph.D. Dissertations	9
IV.	Participating Personnel	9
V.	Inventions	9
VI.	Figure Captions and Figures	10

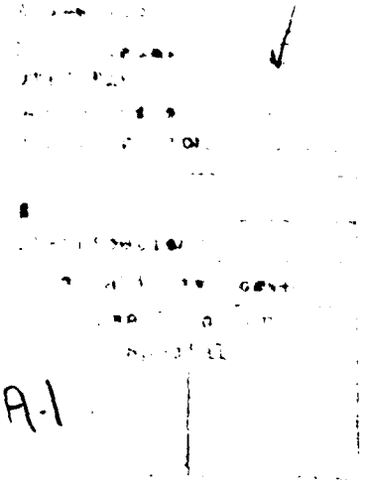

A-1

I. STATEMENT OF THE PROBLEM

Virtually all properties of a solid surface, whether they are physical, chemical, mechanical, or electrical, and all processes that take place on a surface, such as nucleation and growth of single crystals, and adhesion of thin films and coatings, ultimately relate to the atomic and electronic structures of that surface. The invention of the scanning tunneling microscope (STM) by Nobel laureates Gerd Binnig and Heinrich Rohrer has enabled scientists to obtain atomically-resolved images of a surface and by so doing, has completely revolutionized the study of surfaces. STM imaging, until a few years ago, was almost exclusively limited to surfaces of metals, semi-metals and semiconductors. Ceramic surfaces were largely ignored because it was thought that their non-conducting nature would preclude tunneling and imaging would therefore be impossible. We set out to solve the problem of using the STM to obtain atomically resolved images of a ceramic surface. We chose, as our model ceramic, SiC because of its important structural and electronic properties. Our goal was not limited to using the STM merely to obtain images of the surface atoms. We also intended to use the STM to perform spectroscopic measurements on the electronic structure of the surface, and to use the STM to investigate other fundamental problems such as the role of surface defects on the mechanical behavior of the surface under external stresses, the influence of different modes of film growth on the surface topography and its atomic geometry, and the surface reactions between a metal and a ceramic. The last of these problems has led us to conduct a separate experimental and theoretical investigation on the interfacial reactions of the Ti-Si-C system as a precursor to our intended STM study.

II. SUMMARY OF THE MOST IMPORTANT RESULTS

II.1. STM Studies of the β-SiC(100) Surface

The β-SiC(100) single crystals were grown on Si(100) substrates by chemical vapor deposition (CVD) and they were supplied by R. F. Davis of North Carolina State University. The β-SiC(100) surfaces were annealed at

high temperatures, i.e. between 1150 and 1200°C, in ultrahigh vacuum to eliminate the surface oxide prior to tunneling. The samples were nitrogen-doped to a level of ~ 10^{16} cm^{-3} to render them n-type so that tunneling was not a problem.

The STM images showed that the β-SiC(100) surfaces were generally rough and uneven, with a corrugation of ~ 20 Å over 500 Å distances. We attribute the surface undulation to the lattice mismatch between the β-SiC(100) and the Si(100) substrate, i.e. 3.10 Å versus 3.84 Å. Despite the difficulty in obtaining atomically resolved images on such rough surfaces, we were able to observe ordered regions where c(2x2), (3x2) and other large reconstructions took place. Our results were reported in detail in paper #5 on our publication list.

II.2. STM Studies of the β-SiC(111) Surface

The β-SiC(111) single crystals were grown on hexagonal α-SiC{0001} substrates by CVD and they were also supplied by R. F. Davis of NCSU. Two types of β-SiC(111) surfaces were available, one was grown on the Si-terminated α-SiC(0001) surface while the other was grown on the C-terminated α-SiC(000$\bar{1}$) surface. Large scale STM scans showed that the latter was considerably less smooth and contained numerous double-positioning boundaries separating domains with different stacking order. This observation suggests that the lateral epitaxial growth of the β-SiC film on the C-terminated α-SiC(000$\bar{1}$) surface is restricted by the greater activity and higher sticking coefficient on the C-face. As a result, the mobility of the atoms on the surface is decreased and vertical growth dominates. Atomic resolution imaging was not possible on the β-SiC(111) grown on the C-terminated α-SiC(000$\bar{1}$) surface because the corrugations on the domains were greater than the atomic corrugation. These results are discussed in detail in paper #6 on our publication list.

STM imaging with atomic resolution was easily achieved on the β-SiC(111) surface grown on the Si-terminated α-SiC(0001) substrate face. Fig. 1 shows voltage-dependent scans of the same region on a β-SiC(111) surface after a 1200°C annealing treatment to rid the surface of oxides.

The surface shows a 6 x 6 geometry with a unit-cell edge of ~19 Å, which is approximately six times the unit-cell edge of 3.1 Å of the β-

SiC(111)-(1x1) bulk-terminated surface. The images (a) and (b) of Fig. 1 were taken simultaneously on the same area with the tip biased at +3.7V when scanning from left to right and biased at -3.7V when scanning from right to left. The most remarkable feature in these two scans is the occurrence of a contrast reversal. The honeycomb pattern in the filled-state image (a) turns into a centered-hexagon array in the empty-state image (b). The minima of the honeycombs in (a) coincide exactly with the maxima of the centered-hexagons in (b). Each honeycomb minimum and each hexagon maximum has a diameter of ~12 Å, clearly much larger than the size of a single atom. The corrugation of both images was about 0.4 Å.

The spectroscopy of the surface was performed by measuring current-voltage (I-V) dependence under the condition of constant tip-sample separation. This was achieved by holding the voltage on the feedback loop constant for about 150 ms during the acquisition of an I-V curve. Generally, ten I-V curves were collected at the same tip-sample gap and their average taken to give the I-V curve for that gap. From the averaged I-V curves, we plotted (dI/dV)/(I/V) or (dlnI/dlnV) versus V or energy, which has been shown to represent features of the surface density of states (DOS). Fig. 2 shows such a (dI/dV)/(I/V) versus energy curve, giving spectroscopic information of the surface.

Interestingly, our LEED studies of the β-SiC(111) surface annealed at 1200°C showed a $6\sqrt{3}$ x $6\sqrt{3}$ geometry, in agreement with previous LEED experiments by other workers taken on an equivalent α-SiC(0001) surface. The 6 x 6 geometry in STM images was not observed by LEED.

In order to explain why the STM gives a 6 x 6 geometry of the β-SiC(111) surface whereas the LEED gives a $6\sqrt{3}$ x $6\sqrt{3}$ geometry for the same surface, we invoke a model originally proposed by van Bommel and coworkers at Philips Research Laboratories for their LEED studies of the α-SiC(0001) surface. Three successive carbon layers of β-SiC, after the evaporation of silicon by annealing to 1200°C, collapse into one single layer of carbon atoms with a surface density of 3.67×10^{15} atoms cm^{-2}, very close to the density of a graphite monolayer of 3.80×10^{15} atoms cm^{-2}. This layer of carbon atoms then have only to be displaced over small distances to form a graphite layer. Support for the existence of the graphite monolayer can be found in the tunneling spectrum shown in Fig. 2, where peaks at -2.6, 1.3 and 2.5 eV agree with the -2.5 eV π-bonding

state, 1.3 eV π^*-antibonding state, and the 2.5 eV surface state in the surface electronic spectra of graphite calculated theoretically.

In Fig. 3, we have drawn a graphite mesh with periodicity (or unit-cell edge) of 2.46 Å over a Si bulk-terminated (1x1) surface of β-SiC(111) with periodicity of 3.1 Å. The positions where the top C atoms coincide exactly with the Si atoms underneath are marked with circles and labeled A, B, C, D, E and F. These positions give rise to the $6\sqrt{3}$ x $6\sqrt{3}$ geometry observed by LEED since the unit-cell edges, AE and CE, each has a length of 13 graphite hexagons, i.e. 13 x 2.46 Å, which is virtually identical to $6\sqrt{3}$ times 3.1 Å. Around each of the positions A-F, there are three pairs of C and Si atoms at the apexes of the dotted triangle lying very close to each other, i.e. within 0.3 Å laterally. The position G, given by the dotted circle in Fig. 3, does not have any C atoms directly above a Si atom. Six C atoms on the dotted circle, however, are lying very close to six Si atoms. ABGF forms the 6x6 geometry observed by STM. To explain the contrast reversal phenomenon as the tip bias is reversed, we need a detailed knowledge of the electronic structure of the surface.

We have performed first-principles calculations of the electronic structure of the surface shown in Fig. 3. Our calculations, which explain the contrast reversal phenomenon, are summarized in Fig. 4 which shows the partial density of states for the graphite monolayer and those for the Si-terminated surface of β-SiC(111) underneath. Since the work function for the graphite monolayer is smaller than that for the Si-terminated β-SiC(111), there is a net charge transfer from the graphite to the β-SiC. The graphite Fermi level is located at the π band, which is composed solely of P_z orbitals; here z is the coordinate normal to the surface. When there is a Si atom directly beneath or close to a C atom in the graphite layer, i.e. positions A-G in Fig. 3, the charge transfer occurring between these atoms will be maximum, resulting in the increase of the number of empty states of the C atoms. So when the empty states are probed by the negatively-biased tip, the positions A-G appear bright, forming a centered hexagon pattern as in Fig. 1(b). When the tip is biased positively and sampling the filled states, positions A-G appear dark because of the depletion of filled states due to the charge-transfer from the filled states of the C atoms to the Si dangling-bond states underneath. This results in the honeycomb

pattern in Fig. 1(a). Thus the voltage-dependent contrast reversal is explained.

We conclude that the discrepancy between the 6 x 6 STM geometry and the $6\sqrt{3}$ x $6\sqrt{3}$ LEED pattern for the β-SiC(111) surface can be explained by an incommensurate graphite monolayer grown on the Si-terminated β-SiC(111) surface during the annealing process. The contrast reversal phenomenon observed in the STM images at opposite tip biases can be explained by the different electronic contributions from graphite states of those C atoms with Si atoms directly (or almost directly) underneath and those without. The details of our results can be found in papers #7 and #8 in our publication list.

II.3 STM Studies of β-SiC(111) and α-SiC(0001) Surfaces Under External Stresses

An STM with a strain stage was specially built to conduct experiments in which a SiC sample was subjected to an external stress. The sample consisted of a long thin SiC single crystalline wafer clamped at one end. The other free end could be pushed or pulled by small amounts adjusted via a UHV rotary-linear feedthrough. The single crystalline β-SiC(111) and α-SiC(0001) wafer were supplied by Cree Research in North Carolina. Since the application of stress could be finely adjusted, we hoped to observe the initiation of cracking and fracture on an atomic scale on the surface, and the role played by vacancies, dislocations and steps in such a process. Success of the experiment, however, was limited up to the termination date of this project. There were numerous problems in this very delicate experiment and we were just beginning to overcome them. We have no doubt that we will succeed, but we need more time.

II.4 Physical Chemistry and Reaction Chemistry of SiC Ceramics

The thrust of this project from the materials science perspective has been to examine important issues concerning the physical chemistry of silicon carbide-metal alloys and composites. The reason is that the application of silicon carbide as a structural material will likely be in the form of a composite. Consequently, the specific issues that we are

addressing concern the chemical and mechanical compatibility of silicon carbide with the other components. This necessarily involves a detailed examination of interface compatibilities and reactions.

We have focused our investigation principally on the Si-Ti-C system since SiC-TiC and SiC Ti composites hold some promise as high strength-high toughness materials. To a lesser extent, we have studied SiC based composites based on the Si-Al-C-N system. This is of interest due to the capability of forming finely dispersed spinodal-like phase distributions of SiC and AlN, which ultimately contains features desirable for high toughness ceramics.

We undertook a detailed evaluation of the thermochemistry of the Ti-Si-C and Ti-Si-N nitrogen systems by combining reliable information from the literature with our own experimental work directed at clarifying a number of the outstanding inconsistencies existing up to present. We revised the ternary phase diagrams for these systems providing more detail concerning the binary and ternary phase equilibria. However, what was most novel about our work was the construction of the phase stability diagrams and demonstrating how they might be used for interpreting complex series of reactions often seen at reaction interfaces. A stability diagram maps out the stability criteria for each phase of a system in terms of chemical potential (partial molar free energy) and composition space. On this diagram, the reaction paths taken at an interface can be traced allowing a rational analysis of the sequence phases formed. Successive analyses as a function of time and temperature provides sufficient information to provide some predictive power in controlling the reactions.

An example appears in Fig. 5 corresponding to the Ti-Si-C system. The chemical potential of silicon (or rather the activity of silicon where log $a_{Si} = \mu_{Si}/2.303RT$) is plotted as function relative fraction of titanium and silicon. The shaded regions correspond to solid solution phases of significant range of stoichiometry. Horizontal lines represent three phase equilibria and the open fields represent two phase equilibria. The reaction between Ti metal and silicon carbide are followed for two different cases corresponding to different times of reaction. Case II corresponds to relatively short reaction times where at one extreme of no titanium, silicon carbide is stable for log $a_{Si} > 2.0$ and titanium metal is stable at the other extreme at much lower silicon activities. The reaction paths show

intermediate phases of TiC_x and $Ti_5Si_3C_y$ which appear as combinations of layered and mixed phase morphologies. At longer times (Case I), the ternary compound Ti_3SiC_2 appears as a continuous layer adjacent to silicon carbide. This comparison points out that the reaction can be thought of as a dual problem of interdiffusion of Ti with Si and Ti with C. Because carbon diffuses much more rapidly in general than silicon, the reaction zone is gradually but continuously depleted of carbon, thus enriching itself in silicon which is left behind. An increasing silicon activity destabilizes TiC next to silicon carbide to favor the formation of the ternary compound. A continuation of this trend would predict that eventually the silicide phase $TiSi_2$ would form, which is undesirable because of brittleness and poor bonding characteristics. This is indeed what has been found for composite and thin interfaces which have been overannealed. It is interesting to note that the effect of annealing temperature is very similar to that of annealing time, i.e. increasing temperature tends to raise the relative silicon content in the reaction.

We investigated the phase relationships of these reactions (Ti-Si-C system) at pressures up to 20 kbar. Our study was used to demonstrate the effect of nonuniform stresses on phase sequences and morphologies at reaction interfaces. Composites of unusual geometries, or ill-controlled geometries, can give rise to local stresses and stress gradients due to mismatch of thermal expansion coefficients. It was shown for reaction conditions at 1200°C that local compressive stresses could exceed a threshold defining different compatibility relationships phases. For example, high pressures tended to stabilize the phase Ti_3Si which, like other silicides, was undesirable for its bonding characteristics.

Details of this investigation appear in papers #9 and #10 in our publication list.

III. PUBLICATIONS LIST

III.1. Papers published, in press, and submitted.

1. Z.J. Zheng, I.H. Wilson, U. Knipping, D.M. Burt, D.H. Krinsley and I.S.T. Tsong. Atomically Resolved Scanning Tunneling Microscopy Images of Dislocations. Phys. Rev. B38, 12780-12782 (1988).

2. I.H. Wilson, N.J. Zheng, U. Knipping and I.S.T. Tsong. Scanning Tunneling Microscopy of an Ion-Bombarded PbS (001) Surface. Appl. Phys. Lett. 53, 2039-2041 (1988).

3. I.H. Wilson, N.J. Zheng, U. Knipping and I.S.T. Tsong. Scanning Tunneling Microscopy of Ion Impacts on Semiconductor Surfaces. J. Vac. Sci. Technol. A7, 2840-2844 (1989).

4. N.J. Zheng and I.S.T. Tsong. Resonant Tunneling Theory of Imaging Close-packed Metal Surfaces by Scanning Tunneling Microscopy. Phys. Rev. B 41, 2671-2677 (1990).

5. C.S. Chang, N.J. Zheng, I.S.T. Tsong, Y.C. Wang and R.F. Davis. Scanning Tunneling Microscopy of Cubic Silicon Carbide Surfaces. J. Am. Ceram. Soc. 73, 3264-3268 (1990).

6. C.S. Chang, N.J. Zheng, I.S.T. Tsong, Y.C. Wang and R.F. Davis. Studies of β-SiC(001) and (111) Surfaces by Scanning Tunneling Microscopy. J. Vac. Sci. Technol. B9, 681-684 (1991).

7. C.S. Chang, I.S.T. Tsong, Y.C. Wang and R.F. Davis. Scanning Tunneling Microscopy and Spectroscopy of Cubic β-SiC(111) Surfaces. Surface Sci. 256, 354-360 (1991).

8. M.H. Tsai, C.S. Chang, J.D. Dow and I.S.T. Tsong. Electronic Contributions to Scanning Tunneling Microscopy Images of an Annealed β-SiC(111) Surface. Phys. Rev. B (in press).

9. S. Sambasivan and W.T. Petuskey. Thermodynamics of Forming Ti_3SiC_2. J. Am. Ceram. Soc. (submitted).

10. S. Sambasivan and W.T. Petuskey. Phase Relationships in the Ti-Si-C System at High Pressures. J. Mater. Res. (submitted).

11. S. Sambasivan and W.T. Petuskey. Thermochemical Interpretation of Solid State Reactions in the Ti-Si-N System, I. Phase Stability. J. Mater. Res. (submitted).

III.2. Ph.D. Dissertations

1. Jason R. Guth
   Theoretical and Experimental Studies of Silicon Carbide Polytypes and Solid Solution Crystal Structures

2. Nanjiu Zheng
   Scanning Tunneling Microscopy

3. Sankar Sambasivan
   Thermochemistry of Ceramic-Metal Reactions in Ti-Si-N and Ti-Si-C Systems at High Temperatures and Pressures

IV. PARTICIPATING PERSONNEL

I.S.T. Tsong - Principal Investigator

W.T. Petuskey - Co-principal Investigator

C.S. Chang - Postdoctoral Research Associate

J.R. Guth - Graduate Assistant - Ph.D. (1989)

N.J. Zheng - Graduate Assistant - Ph.D. (1990)

S. Sambasivan - Graduate Assistant - Ph.D. (1990)

C.J. Kuo - Graduate Assistant

B.E. Steele - Graduate Assistant

J.L. Stevens - Graduate Assistant

V. INVENTIONS

None

VI. FIGURE CAPTIONS AND FIGURES

Fig. 1 (a) 500 Å x 500 Å filled-state image of the β-SiC(111) surface. V_t = 3.7 V.

(b) 500 Å x 500 Å empty-state image taken simultaneously of the same area as in (a). V_t = -3.7 V.

Fig. 2 A tunneling spectrum, (dI/dV)/(I/V) as a function of energy, of the β-SiC(111) surface. Arrows indicate states associated with graphite.

Fig. 3 A model of a graphite monolayer (represented by honeycombs) incommensurately grown on the (1x1) Si-terminated β-SiC(111) surface (represented by dots). The dashed triangles, denoted by A, B, C, D, E and F, indicate positions where the graphite atoms at the centers of triangles coincide exactly with the Si atoms in the second layer, and those graphite atoms at the apexes almost coincide with the Si atoms underneath. The dashed circle, G, outlines positions where the graphite and Si atoms nearly coincide. The unit cell spacing is 2.46 Å for graphite and 3.1 Å for the (1x1) Si-terminated surface.

Fig. 4 Calculated partial density of states for the Si-terminated surface of β-SiC(111) and for the incommensurately grown graphite monolayer. The Fermi levels with respect to each other are shown below the vacuum level.

Fig. 5 Phase stability diagram for Ti-Si-C system at 1200°C plotting the activity of silicon as a function of the relative concentration of titanium and carbon. The path of compositions and sequence of phases appearing in the reaction zone of Ti-SiC couples are plotted for two different cases. The annealling time for Case I was longer than for Case II.

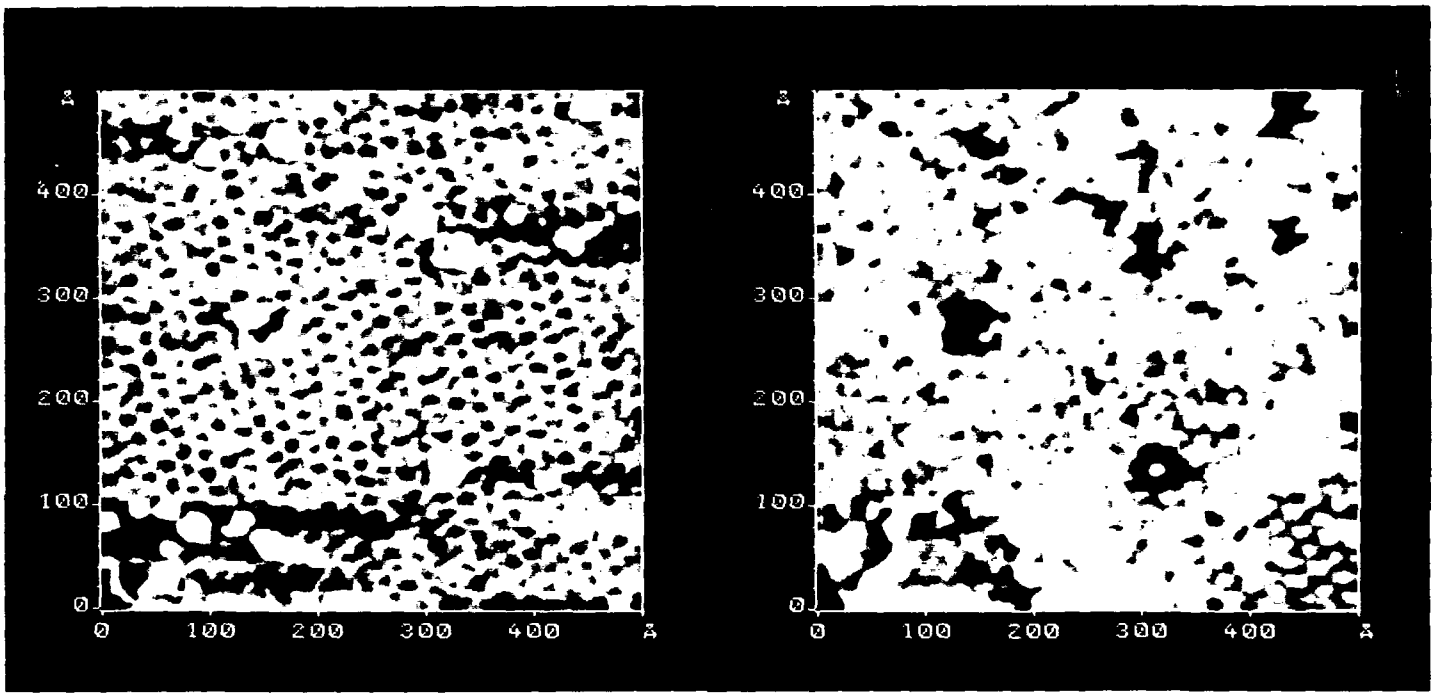
Å
400
300
200
100
0
0
100
200
300
400
Å
Å
400
300
200
100
0
0
100
200
300
400
Å

(a) (b)

Fig. 1

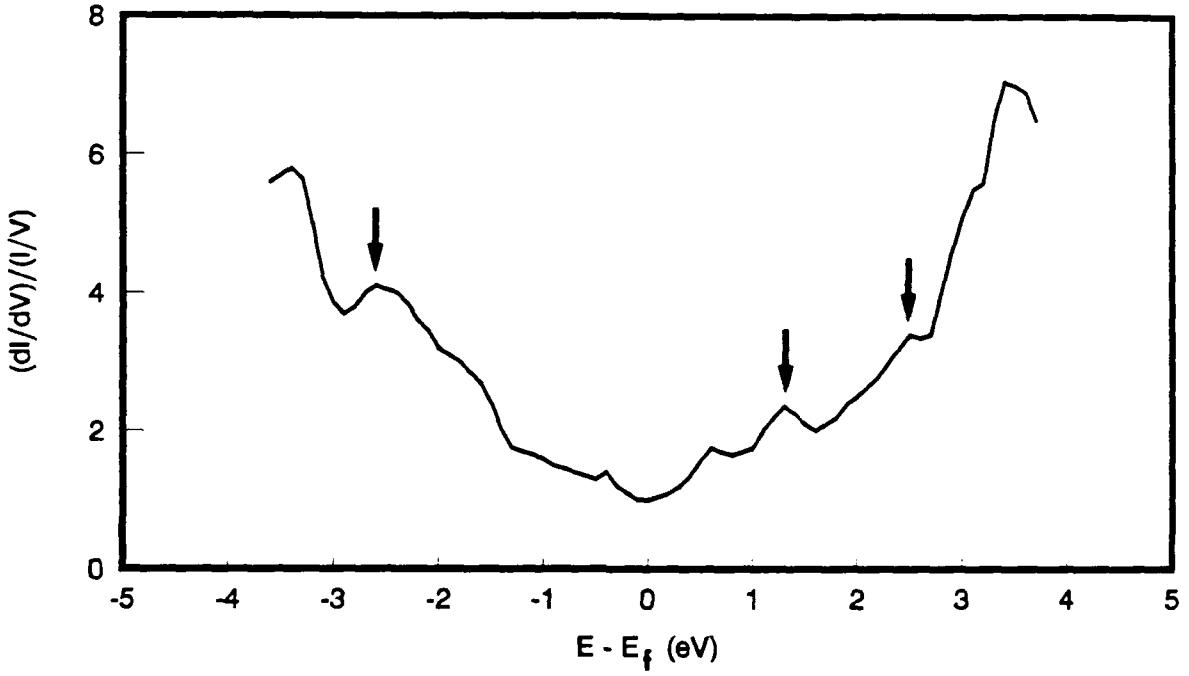

Fig. 2

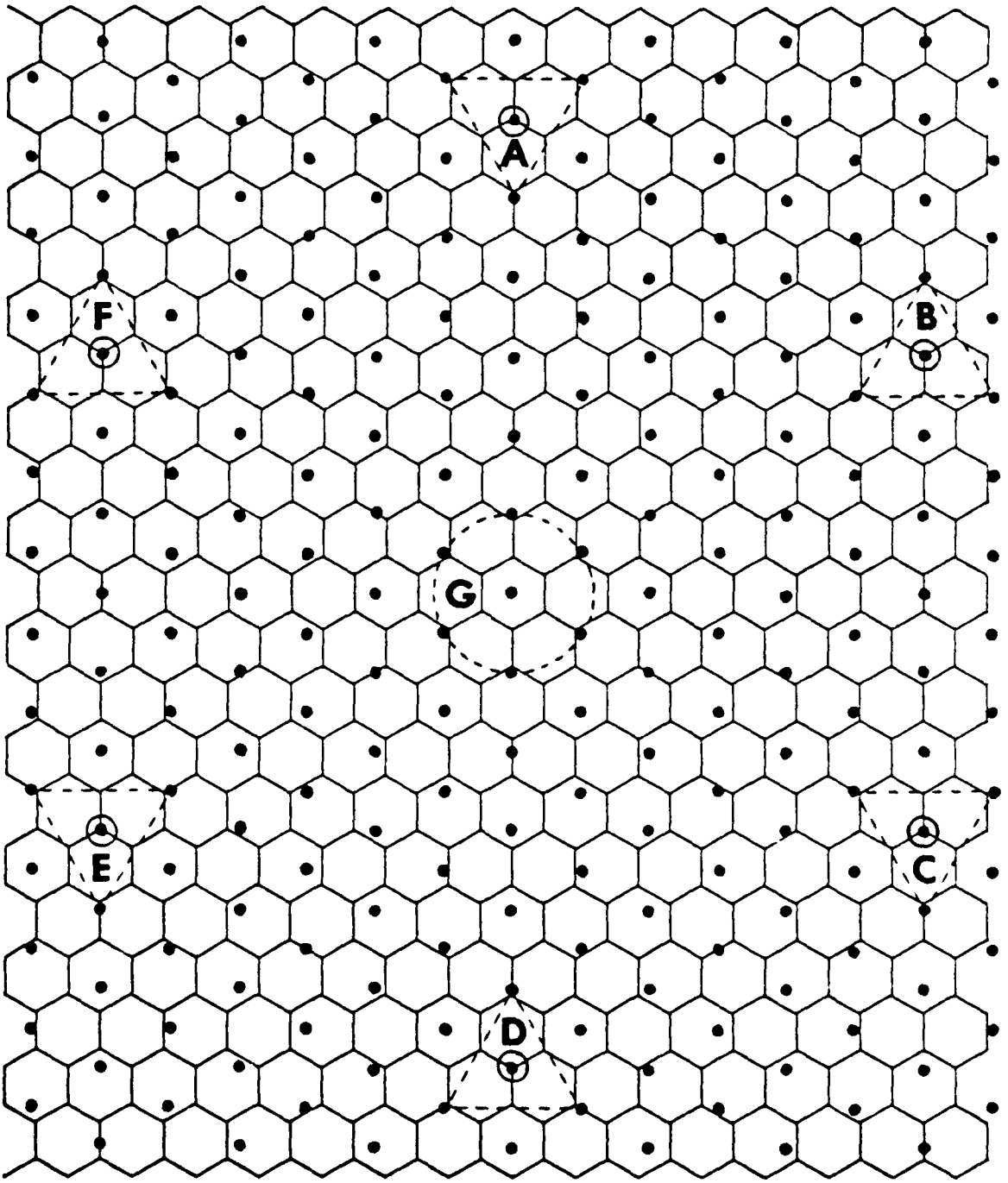

Fig. 3

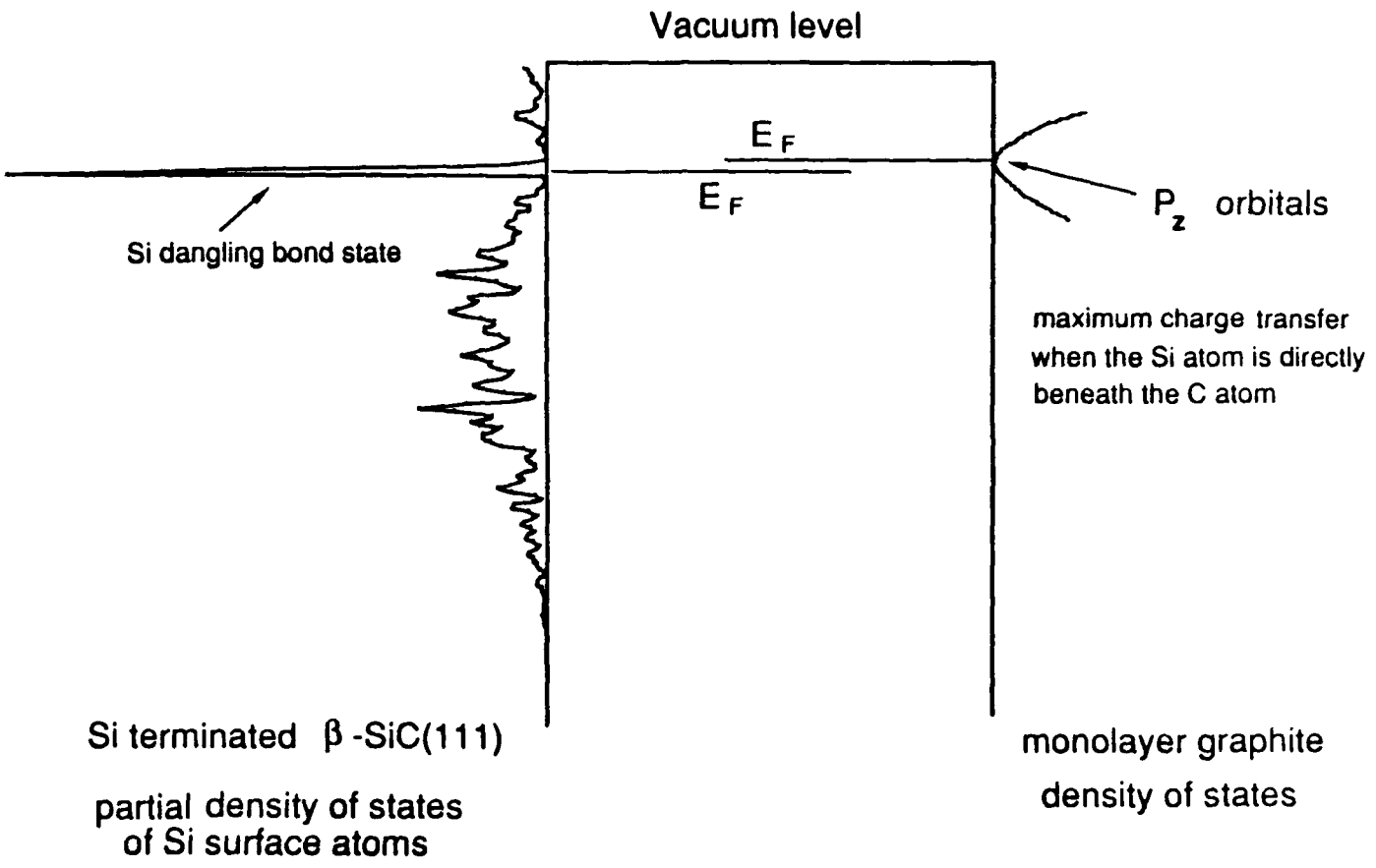
Vacuum level
E_F
E_F
P_z orbitals
Si dangling bond state
maximum charge transfer
when the Si atom is directly
beneath the C atom
Si terminated β -SiC(111)
partial density of states
of Si surface atoms
monolayer graphite
density of states

Fig. 4

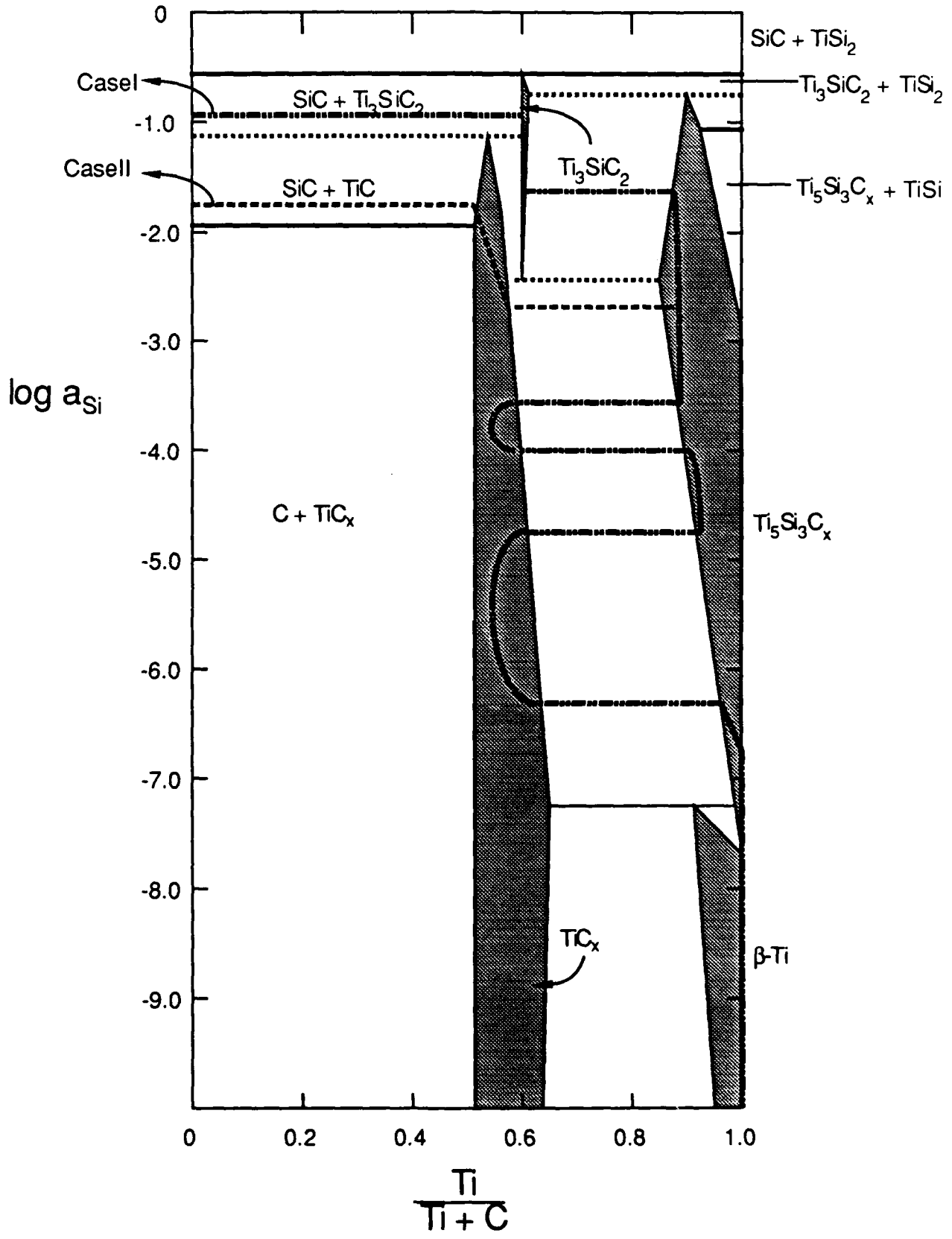
0
-1.0
-2.0
-3.0
-4.0
-5.0
-6.0
-7.0
-8.0
-9.0
log a_{Si}
CaseI
CaseII
SiC + Ti_3SiC_2
SiC + TiC
C + TiC_x
Ti_3SiC_2
TiC_x
SiC + $TiSi_2$
Ti_3SiC_2 + $TiSi_2$
$Ti_5Si_3C_x$ + TiSi
$Ti_5Si_3C_x$
β-Ti
0
0.2
0.4
0.6
0.8
1.0
Ti / (Ti + C)

Fig. 5